

MEASUREMENT OF THE MASS AND STELLAR POPULATION DISTRIBUTION IN M82 WITH THE LBT

JOHNNY P. GRECO, PAUL MARTINI, AND TODD A. THOMPSON

Department of Astronomy, The Ohio State University, Columbus, Ohio 43210, USA; greco.40@buckeyemail.osu.edu

SUBMITTED TO APJ: 2012 JANUARY 25

ABSTRACT

We present a *K*-band spectroscopic study of the stellar and gas kinematics, mass distribution, and stellar populations of the archetypical starburst M82. We used the ¹²CO stellar absorption bandhead at 2.29 μ m (CO_{2,29}) to measure the rotation curve out to nearly 4 kpc radius on both the eastern and western sides of the galaxy. In contrast with the nearly Keplerian gas dynamics suggested by previous measurements of HI and CO emission from the ISM, which imply a truncation in M82's dark matter halo, our data show that the rotation curve is in fact flat on 1 – 4 kpc scales. The kinematics of the Br γ , H₂, and He I emission lines are consistent with, although characterized by slightly higher velocities than, the stellar kinematics. We derived M82's mass distribution from our stellar kinematic measurements and estimate its total dynamical mass is $\sim 10^{10} M_{\odot}$. We measured the equivalent width of CO_{2,29} (*W*_{2,29}) as a function of distance from the center of the galaxy to investigate the spatial extent of the red supergiant (RSG) population. The variation in *W*_{2,29} with radius clearly shows that RSGs dominate the light inside 500 pc radius. M82's famous superwind is likely launched from this region, where we estimate the enclosed mass is $\lesssim 2 \times 10^9 M_{\odot}$.

Subject headings: galaxies: individual (M82) – galaxies: starburst – galaxies: kinematics and dynamics – infrared: galaxies

1. INTRODUCTION

Observations suggest that star formation in galaxies is regulated by feedback processes. In rapidly star-forming galaxies, feedback operates on large scales, driving galaxy-wide superwinds, which can eject the raw materials for future stellar generations if the interstellar material is launched with enough momentum to escape the host galaxy's gravitational potential. Otherwise, the ejected material may be re-accreted in a so-called “fountain flow”. These issues are crucial for understanding the formation of stars in rapidly star-forming galaxies across cosmic time.

The exceptionally high star formation rates present in starburst galaxies make them optimal targets to probe feedback processes. The focus of this paper is the archetype of this class of objects, M82. This galaxy's proximity (3.63 Mpc; $1'' = 17.6$ pc; Freedman et al. 1994; Sakai & Madore 1999; Gerke et al. 2011) and nearly edge-on geometry ($i = 80^\circ$; McKeith et al. 1993) make it a superb laboratory for studying the physics of galactic winds and star formation. At infrared wavelengths, its luminosity is $6 \times 10^{10} L_{\odot}$ (Sanders et al. 2003), which makes it one of the brightest and most observed infrared objects in the sky. Most of its infrared luminosity originates in the starburst core, which is severely obscured by dust at visible and ultraviolet wavelengths (Rieke et al. 1980; Förster Schreiber et al. 2001).

The origin of M82's starburst is thought to be a tidal interaction with its massive companion, M81, $\sim 10^8$ years ago (Gottesman & Weliachew 1977; Lo et al. 1987; Telesco et al. 1991; Achtermann & Lacy 1995). The pronounced HI bridge that connects the galaxies (Cottrell 1977; Yun et al. 1993) is strong evidence for such an interaction. In addition to the dynamical effects associated with tidal forces from M81, the global dynamics and evolution of the starburst are further perturbed by the presence of a stellar bar (Telesco et al. 1991), which may have formed as a result of the interaction.

As an interacting, barred galaxy, M82's observed dynamical properties are distinct from those seen in typical Sb and Sc

galaxies. Molecular gas measurements by Young & Scoville (1984) show that the CO velocity field contains warps and peculiarities that are consistent with a significant non-circular velocity component, perhaps due to radial infall or a polar ring tilted with respect to the major axis. In addition, measurements of CO (2,1) by Sofue et al. (1992) suggest that the rotation of the gas disk is nearly Keplerian at radii > 1 kpc. Sofue (1998) reproduced this Keplerian motion with a model in which the outer disk and halo were stripped during the encounter with M81. Although flat rotation curves are observed in the vast majority of galaxies, Rubin & Ford (1982) found falling rotation curves in several tidally interacting galaxies, which suggests that some dark matter is stripped from galaxies during interactions.

Förster Schreiber et al. (2003) proposed that M82's starburst activity occurred in two successive episodes that each lasted a few million years and peaked about 10^7 and 5×10^6 years ago. In this model, the encounter with M81 triggered the first burst in the central 500 pc by inducing strong large-scale torques, loss of angular momentum, and an infall of molecular clouds towards the nuclear region. The second burst occurred in a circumnuclear ring and along the stellar bar, and is attributed to bar-induced dynamical resonances. The Förster Schreiber et al. (2003) starburst model can explain the apparent abundance of red supergiants (RSGs) that dominate the light within 500 pc radius.

In order to understand the dynamics of the ejected gas and constrain the physics of feedback processes in M82, it is essential to accurately measure the total dynamical mass on both the small scales of star-forming regions and the large scales of the entire galaxy. Rotation curves are the major tool for determining the distribution of mass in galaxies (Sofue & Rubin 2001), and many studies have employed gas and stellar kinematics at a range of wavelengths to measure radial velocities in M82 (e.g. Saito et al. 1984; Goetz et al. 1990; McKeith et al. 1993; Achtermann & Lacy 1995; Sofue et al. 1992). Greve (2011) includes a compilation

of these results. Given that M82 has recently undergone tidal interactions and harbors an extraordinary superwind, stellar kinematics should be a more reliable tracer of the mass distribution than the gas. Nearly all previous stellar kinematic measurements used visible-wavelength tracers, which may be compromised by the substantial dust attenuation present in the galaxy. The near-infrared K -band is a better tracer of the stellar kinematics, as attenuation in the K -band is approximately a factor of ten less than in the V -band. In this study, we use K -band spectroscopy to study M82's gas and stellar kinematics, mass distribution, and stellar populations.

2. OBSERVATIONS AND DATA REDUCTION

We obtained K -band spectra of M82 at the Mount Graham International Observatory with the LUCI-1 spectrograph and the Large Binocular Telescope (LBT) on 2011 February 10. The observations were made through a K -band filter (2.05–2.37 μm) with the N1.8 camera, which has a plate scale of $0''.25 \text{ pixel}^{-1}$ and a field of view of $4' \times 4'$. A grating with 210 lines mm^{-1} was used with a slit width of $1''$. This combination yields a spectral resolution of $\lambda/\Delta\lambda \approx 3,000$ or 100 km s^{-1} . Two slit positions, which we designate as M82E and M82W, were used to measure the rotation curve out to $4'$ ($\sim 4 \text{ kpc}$) from the center of the galaxy. We centered each end of the slit on the nuclear region at a position angle of 67.5° (Figure 1). The observations were made with 300 second exposures in an *object-sky* sequence for a total on-source integration time of 1 hour per slit position. A telluric standard close in air mass to M82 was observed before and after both the M82E and M82W observations.

We carried out standard data reduction within the IRAF¹ software package. The two-dimensional data were transformed onto an orthogonal wavelength/slit-position grid based on a wavelength solution from the sky's bright OH emission lines. This transformation linearized the dispersion to $\sim 1.64 \text{ \AA pixel}^{-1}$. We used the *xtellcor* (Vacca et al. 2003) package within IDL to correct for absorption from the Earth's atmosphere. The telluric standard spectra had slightly higher spectral resolution than was obtained for M82. This is likely because the light from the stars did not fill the $1''$ wide slit. This complication was remedied by convolving the telluric spectra with Gaussians to match their resolutions to M82.

3. ROTATION CURVE

To measure the rotation curve, we symmetrically extracted thirty apertures each from the M82E and M82W slit positions. We progressively increased the bin sizes at larger radii to achieve a sufficient signal-to-noise ratio in the stellar continuum. Figure 2 shows illustrative K -band spectra from M82's nucleus and eastern side. We measured the rotation curve out to nearly 4 kpc radius with the ^{12}CO stellar absorption bandhead at $2.29 \mu\text{m}$ ($\text{CO}_{2,29}$) and to $\sim 1 \text{ kpc}$ radius with gas emission (He I , H_2 , $\text{Br}\gamma$) from the interstellar medium. Because of the extreme tidal forces and galactic wind in M82, the gas and stars may trace distinct kinematic structures, and we discuss each in turn.

3.1. Stellar Absorption

¹ IRAF is distributed by the National Optical Astronomy Observatory, which is operated by the Association of Universities for Research in Astronomy, Inc., under cooperative agreement with the National Science Foundation.

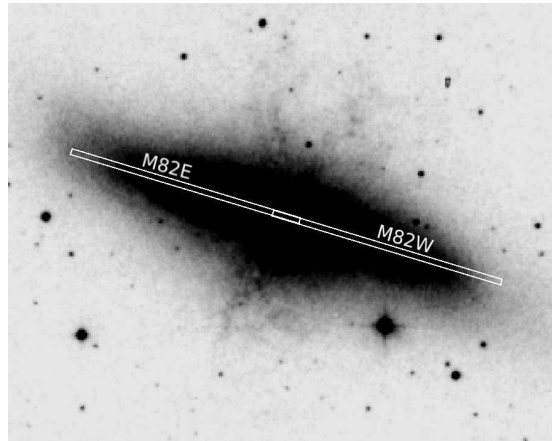


FIG. 1.— Digital Sky Survey image of M82 with overlays of our two slit positions. Each slit is $4'$ long and they overlap on the center of the galaxy. The widths of the slits have been increased by a factor of six for ease of visibility in this figure.

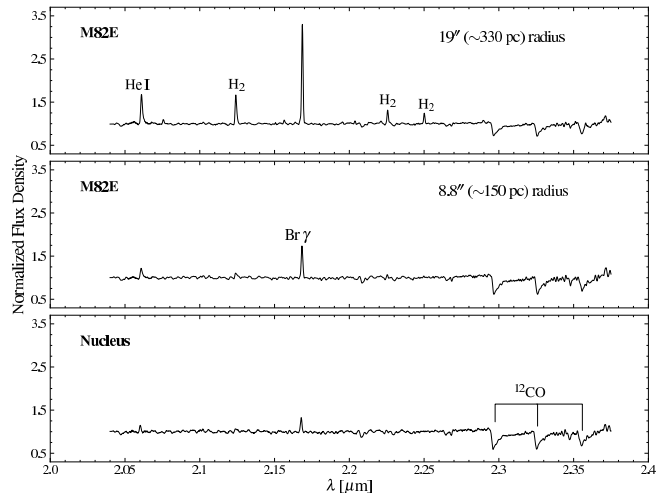


FIG. 2.— K -band spectra from M82's nucleus, $8.8''$ east from center, and $19''$ east from center. $\text{CO}_{2,29}$, which is the dominant absorption feature, originates in the atmospheres of cool, evolved stars. The He I and $\text{Br}\gamma$ lines trace star formation, and the H_2 is evidence of shocked gas. The strength of the emission lines peaks near $19''$.

$\text{CO}_{2,29}$ originates in the atmospheres of cool, evolved stars and provides a strong absorption feature for stellar velocity measurements (e.g. Gaffney et al. 1995). Previous studies of M82 have used $\text{H}\alpha$ and NaD to measure the rotation curve with stellar kinematics (e.g. Mayall 1960; Goetz et al. 1990), yet these measurements are likely compromised by the $A_V \sim 5 \rightarrow 25$ attenuation toward the central region (Rieke et al. 1980; Lester et al. 1990; Puxley 1991). At somewhat longer wavelengths, McKeith et al. (1993) measured the stellar kinematics with Ca II stellar absorption lines (8662, 8542, 8498 \AA). If the near-infrared extinction wavelength dependence is given by the relation $A_\lambda \propto \lambda^{-1.75}$ (Draine 1989), attenuation for $\text{CO}_{2,29}$ is approximately a factor of five less than Ca II . With the copious amount of gas and dust present, an improvement at this level may reveal kinematic features that are otherwise obscured.

To measure the stellar rotation curve, we selected six apertures with high signal-to-noise as cross-correlation templates for relative velocity measurements. We used the *rvsao* pack-

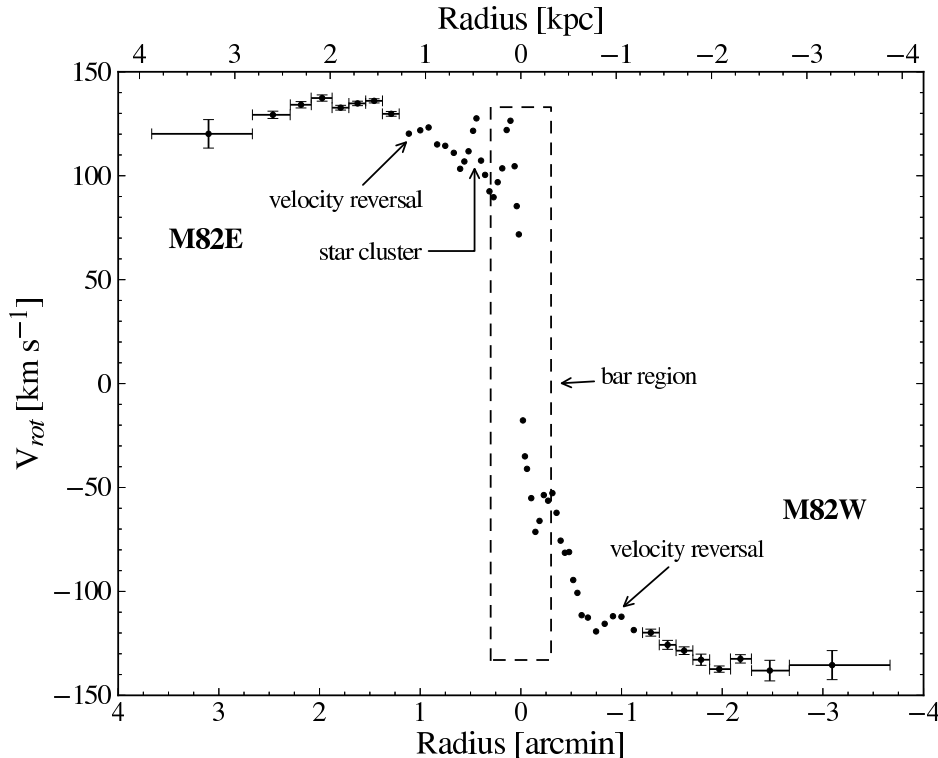


FIG. 3.— Stellar rotation curve based on CO_{2.29}. The horizontal error bars indicate the aperture size of the measurement, and the vertical error bars represent the uncertainty of the velocity measurement. All data points without error bars have uncertainties less than 2 km s⁻¹ and aperture sizes less than 5". The flatness of the rotation curve is inconsistent with Keplerian motion. The symmetric, sharp features on either side of the nucleus are due to the non-circular motions of the stellar bar. At ~1 kpc on either side of the galaxy, there is an apparent “velocity reversal”, which may be due to symmetric spiral arms.

age within IRAF to cross-correlate all sixty apertures against each of the six templates. We restricted the wavelength range from 2.28 to 2.365 μm to focus the analysis on CO_{2.29}. This resulted in six independent rotation curves, all of which we normalized to be symmetric around zero velocity. After correcting for M82’s nearly edge-on inclination, we took the mean velocity at each point to be the value of the rotation curve at that point, and the uncertainty was calculated as the rms between the six curves. Figure 3 shows our stellar rotation curve. The horizontal bars represent aperture size. All data points without error bars have uncertainties less than 2 km s⁻¹ and aperture sizes less than 5". Table 1 lists the measurements (apertures selected as cross-correlation templates are marked with a dagger).

The observed stellar velocities show the stellar rotation curve is flat on scales of 1 – 4 kpc. This is in stark contrast with the nearly Keplerian gas dynamics suggested by H I and CO emission from the interstellar medium (Sofue et al. 1992). The gas, however, is severely disrupted by the wind and may also be affected by radial inflow and tides (Young & Scoville 1984). The stellar data are therefore expected to trace the mass distribution much more reliably.

The rotation curve for M82E appears to decline slightly from $\sim 2 \rightarrow 4$ kpc. This decline has $\sim 2\sigma$ significance and may be due to tidal stripping caused by the interaction with M81. The declining rotation curve is at the approximate location of a flaring in the stellar disk and the northern H I streamer (Yun et al. 1993). No decline is seen in the M82W data. Measurements at larger radii are needed to determine whether or not the falloff is due to tidal stripping.

Telesco et al. (1991) discovered M82’s stellar bar with observations at infrared wavelengths and estimated it to be ap-

proximately 1 kpc in length. Numerical simulations have shown that galaxy interactions are effective at inducing galactic bars (e.g. Noguchi 1988; Miwa & Noguchi 1998), and the strong evidence for past tidal interaction observed in M82 makes it an excellent testing ground for theories of bar formation. Although it is difficult to observationally determine the origin of M82’s bar, the effects of its presence can be seen in our stellar rotation curve as the symmetric, sharp features on either side of the nucleus.

The second bump at ~ 500 pc may be the result of a super star cluster (seen in the two-dimensional data) that fell on the slit. This cluster, which was identified as J0955548+694953 by McCrady et al. (2003), likely dominates the flux from this aperture, and its velocity excess with respect to the main rotation curve likely indicates strong non-circular motion. However, it is puzzling that multiple points define the feature and that no other studies have seen this second peak in the rotation curve. Other possible explanations for the feature are the presence of tightly wound spiral arms and patchy *K*-band extinction.

Our data contain evidence of a “velocity reversal” (velocity decrease) at ~ 1.0 kpc on both the eastern and western sides of the galaxy. Greve (2011) highlights the existence of a 100 km s⁻¹ velocity reversal of gas and/or stars at ~ 1.0 kpc in H δ and H ϵ stellar absorption on the eastern side of the galaxy, as well as in ionized gas emission lines at visible and blue wavelengths on the eastern and western sides; interestingly, the feature is apparently absent in near-infrared Ca II stellar absorption. Although the velocity amplitude of our detection is approximately a factor of ten less, the reversal is present in our data. Local extinction is not likely to be the culprit, as the feature is symmetric with respect to the nu-

TABLE 1
STELLAR ROTATION CURVE DATA

M82E				M82W			
Position (arcmin)	Aperture (arcmin)	Velocity (km/s)	Uncertainty (km/s)	Position (arcmin)	Aperture -1 × (arcmin)	Velocity (km/s)	Uncertainty (km/s)
0.0203	0.0125 - 0.0292	71.8	1.8	-0.0205	0.0125 - 0.0292	-17.7	1.3
0.0411	0.0333 - 0.0500 [†]	85.4	1.9	-0.0403	0.0333 - 0.0500 [†]	-35.0	1.2
0.0622	0.0417 - 0.0833	104.6	1.7	-0.0609	0.0417 - 0.0833	-41.0	1.2
0.1034	0.0833 - 0.1250	126.5	1.2	-0.1031	0.0833 - 0.1250	-55.1	1.0
0.1412	0.1250 - 0.1667	122.0	1.2	-0.1443	0.1250 - 0.1667	-71.4	0.8
0.1848	0.1667 - 0.2083	103.6	1.7	-0.1851	0.1667 - 0.2083	-66.1	2.0
0.2303	0.2083 - 0.2500	96.9	1.4	-0.2278	0.2083 - 0.2500	-53.6	2.7
0.2711	0.2500 - 0.2917	89.7	1.3	-0.2706	0.2500 - 0.2917	-56.4	2.2
0.3121	0.2917 - 0.3333	92.5	1.0	-0.3133	0.2917 - 0.3333	-52.7	1.7
0.3553	0.3333 - 0.3750	100.4	1.0	-0.3542	0.3333 - 0.3750	-62.2	1.8
0.3955	0.3750 - 0.4167	107.3	1.3	-0.3950	0.3750 - 0.4167	-75.6	1.7
0.4413	0.4166 - 0.4583	127.6	1.2	-0.4372	0.4166 - 0.4583	-81.4	1.6
0.4747	0.4583 - 0.5000	121.6	1.0	-0.4789	0.4583 - 0.5000	-81.0	1.7
0.5198	0.5000 - 0.5417	111.8	1.2	-0.5200	0.5000 - 0.5417	-94.5	1.4
0.5614	0.5416 - 0.5833	106.9	1.3	-0.5615	0.5416 - 0.5833	-100.7	1.4
0.6032	0.5833 - 0.6250 [†]	103.3	1.8	-0.6037	0.5833 - 0.6250 [†]	-111.4	1.9
0.6662	0.6250 - 0.7083	111.0	1.5	-0.6657	0.6250 - 0.7083	-112.6	1.7
0.7512	0.7083 - 0.7917	114.4	1.5	-0.7471	0.7083 - 0.7917	-119.3	1.4
0.8318	0.7916 - 0.8750	115.1	1.8	-0.8325	0.7916 - 0.8750	-115.6	1.7
0.9166	0.8750 - 0.9583 [†]	123.2	1.6	-0.9149	0.8750 - 0.9583 [†]	-111.9	1.9
0.9994	0.9583 - 1.0416	121.9	1.3	-0.9990	0.9583 - 1.0416	-112.2	1.8
1.1127	1.0416 - 1.2083	120.3	1.2	-1.1217	1.0416 - 1.2083	-118.6	1.8
1.2876	1.2083 - 1.3750	129.8	1.1	-1.2908	1.2083 - 1.3750	-119.8	1.7
1.4572	1.3750 - 1.5417	136.0	1.0	-1.4576	1.3750 - 1.5417	-125.7	2.2
1.6221	1.5417 - 1.7083	134.8	1.1	-1.6220	1.5417 - 1.7083	-128.5	1.8
1.7900	1.7083 - 1.8750	132.7	1.1	-1.7897	1.7083 - 1.8750	-132.9	2.7
1.9741	1.8750 - 2.0833	137.4	1.5	-1.9705	1.8750 - 2.0833	-137.4	1.5
2.1838	2.0833 - 2.2917	134.1	1.5	-2.1801	2.0833 - 2.2917	-132.4	2.0
2.4630	2.2917 - 2.6667	129.3	1.8	-2.4728	2.2917 - 2.6667	-138.1	5.0
3.1024	2.6667 - 3.6667	120.2	6.9	-3.0919	2.6667 - 3.6667	-135.5	7.0

NOTE. — All values are measured with respect to M82's center. The positions are flux weighted. At M82's distance, $1'' \approx 1.056$ kpc.

[†] Cross-correlation aperture

cleus. Greve (2011) investigates the hypothesis that the reversal is due to local surface density enhancements associated with spiral arms (Mayya et al. 2005), but finds inconsistencies with this picture. For instance, the absence of the velocity reversal in near-infrared Ca II stellar absorption suggests that it is not inherent to the disk, and the blue-wavelength detections of the eastern velocity reversal reach negative velocities, which cannot be explained from the rotation of a stellar disk with embedded corotating spiral arms. Nevertheless, the detection of the reversal in ^{12}CO stellar absorption and the symmetry about the nucleus indicate the feature is present in the stellar population and implies it is due to a local density enhancement, such as spiral arms.

3.2. Gas Emission

There are several prominent gas emission lines in our data that are characteristic of starburst activity, most notably $\text{Br}\gamma$, HeI , and H_2 (Figure 2). The $\text{Br}\gamma$ and HeI are recombination lines that trace photoionized nebulae, and the H_2 is a rovibrational line that traces shocked gas. In contrast to the observed strength of $\text{CO}_{2,29}$ relative to the continuum, which decreases with distance from the nucleus, the emission lines show an increase of intensity with distance inside 350 pc radius and a rapid decrease with distance beyond 1 kpc radius. This is consistent with the intensity variations measured by Förster Schreiber et al. (2001).

For each aperture listed in Table 1 with sufficient signal-to-noise, we used the `emsao` package within IRAF to measure the velocity offset of each emission line relative to its

rest wavelength (Cox 2000). We normalized the emission line rotation curves to the $\text{CO}_{2,29}$ velocity in an aperture $\sim 1.25''$ west of the nucleus. Figure 4 compares our gas and stellar rotation curves with the nearly Keplerian gas dynamics measured in CO (2,1) by Sofue (1998). The emission lines used to measure the gas kinematics are only detected out to 1 kpc.

On average, our measurements show that the gas moves with higher velocities than the stars inside 1 kpc. This can be explained by forces from the stellar bar, which tend to drive the gas towards the center of the galaxy. Sofue (1998) measured even larger velocities with radio observations of CO (2,1) and HI in this region. Measurements of optical OII emission from ionized gas by McKeith et al. (1993), on the other hand, yielded lower velocities than the stars. As the depth of an observation is a function of wavelength, these discrepancies may be the result of optical depth variations.

4. MASS DISTRIBUTION

The mass of M82 has a much larger contribution from atomic and molecular gas than seen in typical spiral galaxies. Young & Scoville (1984) estimate that between 30% and 40% of the galaxy's mass is in the ISM and that the H_2/HI mass ratio is approximately 10:1. These authors postulate that the high gas fraction may be due to infalling material that contributes to the available reservoir. The estimated dynamical mass of M82 ranges from several times $10^9 \rightarrow 10^{10} M_\odot$ in the literature (e.g. Burbidge et al. 1964; Crutcher et al. 1978; Young & Scoville 1984; Goetz et al. 1990; Sofue et al. 1992); however, the substantial dust attenuation and non-circular mo-

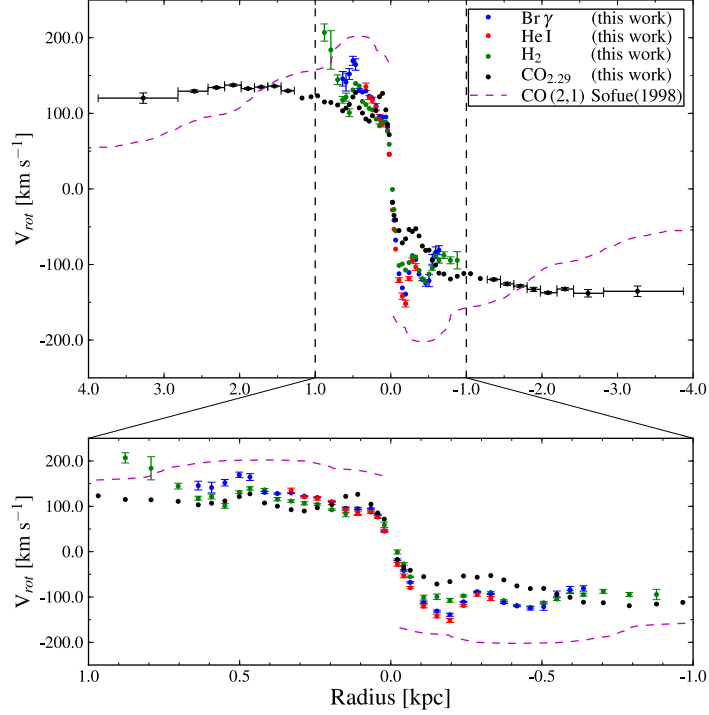


FIG. 4.— The gas and stellar rotation curves from this work with the nearly Keplerian measurements of CO (2,1) by Sofue (1998). The bottom panel is a magnification of the dashed region in the top panel. On average, the gas has larger velocities than the stars. The stellar rotation curve is not consistent with Keplerian motion.

tions associated with tidal forces and the stellar bar make the estimation of the mass challenging and uncertain.

Figure 5 shows the mass profile based on our stellar kinematic measurements. Similar to the studies mentioned above, we assumed circular motion to calculate the enclosed mass at each point. While non-circular motions are expected in the central region, and in particular in the bar region, circular motion is a good assumption at large scales. At 4 kpc the mass distribution appears to be asymptotically approaching $\sim 10^{10} M_{\odot}$. This is likely the total mass of the galaxy, as these measurements are based on stellar motions and extend out to nearly 4 kpc from the nucleus.

Circular motion is not a good assumption in the central region, where the bar and perhaps other asymmetries in the potential produce non-circular motions. Nevertheless, here we estimate the mass within 500 pc is $\lesssim 2 \times 10^9 M_{\odot}$, which is consistent with mass measurements of this region by Young & Scoville (1984), Goetz et al. (1990), and Greve et al. (2002). This mass estimate may be high by a factor of two based on the mass distribution for M82E and M82W shown in Figure 5.

5. STELLAR POPULATIONS

The CO absorption index in stars increases with increasing stellar luminosity, decreasing effective temperature, and increasing metallicity (Frogel et al. 1978, 1983). Large CO indices are indicative of either a stellar population dominated by RSGs or one dominated by old, metal-rich giants. These two possibilities have led to much debate on the nature of M82’s evolved stellar population, particularly in the nucleus (Förster Schreiber et al. 2001). Starburst models with RSG-dominated nuclei, however, provide the best fit to the observed properties of M82 (Rieke et al. 1993; Förster Schreiber et al. 2003).

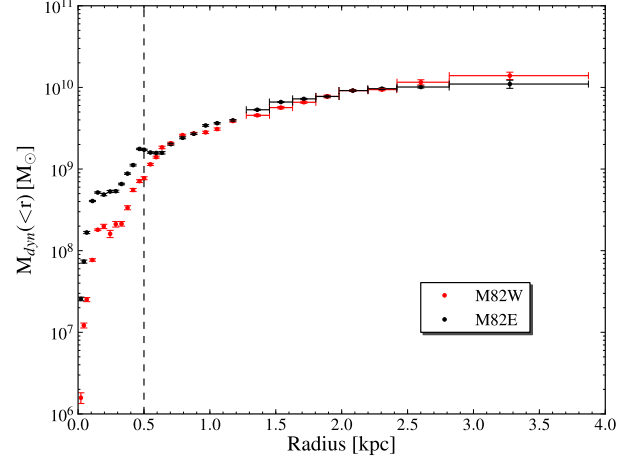


FIG. 5.— Mass profile derived from our stellar rotation curve. Circular motion was assumed in the derivation. The horizontal error bars denote the aperture size of the measurement. The apparent decrease in mass at short radii may be due to the non-circular motions associated with the stellar bar. The superwind is likely launched from the region inside the dashed line, where we estimate the mass is $\lesssim 2 \times 10^9 M_{\odot}$.

Our data reveal very deep CO absorption in M82’s starburst core. In Figure 6, we show the equivalent width of CO_{2,29} ($W_{2,29}$) as a function of radius. The data clearly show a significant increase in $W_{2,29}$ within 500 pc radius. Based on the diagnostic diagrams proposed by Origlia et al. (1993) and Oliva et al. (1995), these results suggest that RSGs dominate the near-infrared continuum throughout the starburst core. At yet smaller radii, Förster Schreiber et al. (2001) found that $W_{2,29}$ within the central 35 pc is characteristic of RSGs with $T_{\text{eff}} = 3600 - 4200$ K.

The dramatic contrast in $W_{2.29}$ between the starburst core and the stellar disk can be explained by the successive starburst model proposed by Förster Schreiber et al. (2003), in which the disk and the starburst core are composed of two distinct stellar populations.

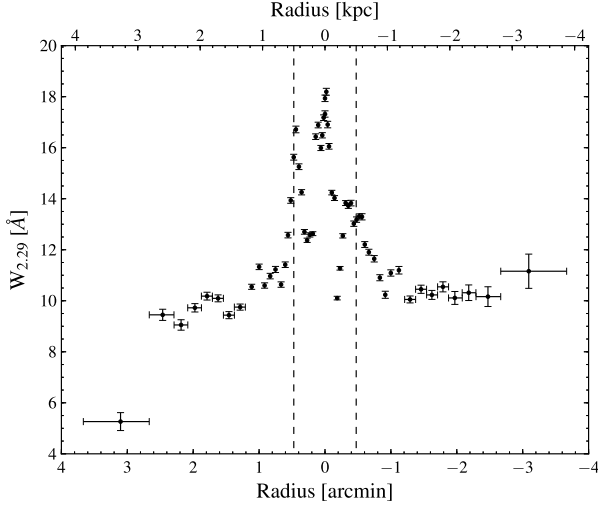


FIG. 6.— $W_{2.29}$ as a function of distance from the center of the galaxy. The horizontal error bars indicate the aperture size of the measurement. The peak in $W_{2.29}$ inside the dashed region is indicative of a stellar population dominated by RSGs.

6. SUMMARY

We have used longslit, K -band spectroscopy from the LBT to measure the stellar and gas kinematics and study the mass and stellar population distribution in M82. The primary points

of this paper can be summarized as follows.

We used ^{12}CO stellar absorption to measure the rotation curve out to nearly 4 kpc on the eastern and western sides of the galaxy. While previous measurements of HI and CO from the interstellar medium suggested that M82’s rotation curve is Keplerian, our data show that it is flat on scales of 1 – 4 kpc (Figure 3). The rotation curve also contains the signatures of the stellar bar and an apparent “velocity reversal” at ~ 1.0 kpc on either side of the galaxy that may be the manifestation of symmetric spiral arms.

We measured the rotation curve with the $\text{Br}\gamma$, He I, and H_2 emission lines from the interstellar medium out to 1 kpc from the nucleus. These gas rotation curves have velocities 10 – 50 km s^{-1} greater than the stellar velocities (Figure 4). The gas dynamics are expected to be disrupted more than the stars by the presence of tides and galactic winds, and may thus be a less accurate tracer of the total mass distribution.

We used the stellar absorption data to measure the mass distribution (Figure 5) and investigate the stellar populations as a function of radius (Figure 6). We estimate the total dynamical mass of M82 is $\sim 10^{10} M_{\odot}$. The strong variation in $W_{2.29}$ with radius clearly indicates that the starburst is located within the central 500 pc radius. The superwind is likely launched from this region, and we estimate its mass is $\lesssim 2 \times 10^9 M_{\odot}$. This mass estimate is somewhat uncertain due to the presence of non-circular motions, but nevertheless provides an upper limit to the gravitational potential of the starburst region.

We are grateful to Jeff Blackburne and Jill Gerke for taking the data as part of the OSU/RC queue. JPG is grateful for support from an undergraduate research scholarship from the College of Arts and Sciences at the Ohio State University. PM is grateful for support from the NSF via award AST-0705170. TAT is supported in part by NASA grant NNX10ADOIG and an Alfred P. Sloan fellowship.

REFERENCES

- Achtermann, J. M., & Lacy, J. H. 1995, *ApJ*, 439, 163
 Burbidge, E. M., Burbidge, G. R., & Rubin, V. C. 1964, *ApJ*, 140, 942
 Cottrell, G. A. 1977, *MNRAS*, 178, 577
 Cox, A. N. 2000, *Allen’s Astrophysical Quantities*, 4th ed.
 Crutcher, R. M., Rogstad, D. H., & Chu, K. 1978, *ApJ*, 225, 784
 Draine, B. T. 1989, *Infrared Spectroscopy in Astronomy*, 290, 93
 Förster Schreiber, N. M., Genzel, R., Lutz, D., Kunze, D., & Sternberg, A. 2001, *ApJ*, 552, 544
 Förster Schreiber, N. M., Genzel, R., Lutz, D., & Sternberg, A. 2003, *ApJ*, 599, 193
 Freedman, W. L., et al. 1994, *ApJ*, 427, 628
 Frogel, J. A., Persson, S. E., Matthews, K., & Aaronson, M. 1978, *ApJ*, 220, 75
 Frogel, J. A., Persson, S. E., & Cohen, J. G. 1983, *ApJS*, 53, 713
 Gaffney, N. I., Lester, D. F., & Doppmann, G. 1995, *PASP*, 107, 68
 Gerke, J. R., Kochanek, C. S., Prieto, J. L., Stanek, K. Z., & Macri, L. M. 2011, *arXiv:1103.0549*
 Goetz, M., Downes, D., Greve, A., & McKeith, C. D. 1990, *A&A*, 240, 52
 Gottesman, S. T., & Weliachew, L. 1977, *ApJ*, 211, 47
 Greve, A., Wills, K. A., Neininger, N., & Pedlar, A. 2002, *A&A*, 383, 56
 Greve, A. 2011, *A&A*, 529, A51
 Lester, D. F., Carr, J. S., Joy, M., & Gaffney, N. 1990, *ApJ*, 352, 544
 Lo, K. Y., Cheung, K. W., Masson, C. R., et al. 1987, *ApJ*, 312, 574
 Mayall, N. U. 1960, *Annales d’Astrophysique*, 23, 344
 Mayya, Y. D., Carrasco, L., & Luna, A. 2005, *ApJ*, 628, L33
 McKeith, C. D., Castles, J., Greve, A., & Downes, D. 1993, *A&A*, 272, 98
 McCrady, N., Gilbert, A. M., & Graham, J. R. 2003, *ApJ*, 596, 240
 Miwa, T., & Noguchi, M. 1998, *ApJ*, 499, 149
 Noguchi, M. 1988, *A&A*, 203, 259
 Oliva, E., Origlia, L., Kotilainen, J. K., & Moorwood, A. F. M. 1995, *A&A*, 301, 55
 Origlia, L., Moorwood, A. F. M., & Oliva, E. 1993, *A&A*, 280, 536
 Puxley, P. J. 1991, *MNRAS*, 249, 11P
 Rieke, G. H., Lebofsky, M. J., Thompson, R. I., Low, F. J., & Tokunaga, A. T. 1980, *ApJ*, 283, 24
 Rieke, G. H., Loken, K., Rieke, M. J., & Tamblyn, P. 1993, *ApJ*, 412, 99
 Rubin, V. C., & Ford, W. K., Jr. 1982, *BAAS*, 14, 949
 Saito, M., Sasaki, M., Kaneko, N., Nishimura, M., & Toyama, K. 1984, *PASJ*, 36, 305
 Sakai, S., & Madore, B. F. 1999, *ApJ*, 526, 599
 Sanders, D. B., Mazzarella, J. M., Kim, D.-C., Surace, J. A., & Soifer, B. T. 2003, *AJ*, 126, 1607
 Sofue, Y. 1998, *PASJ*, 50, 227
 Sofue, Y., Reuter, H.-P., Krause, M., Wielebinski, R., & Nakai, N. 1992, *ApJ*, 395, 126
 Sofue, Y., & Rubin, V. 2001, *ARA&A*, 39, 137
 Telesco, C. M., Campins, H., Joy, M., Dietz, K., & Decher, R. 1991, *ApJ*, 369, 135
 Vacca, W. D., Cushing, M. C., & Rayner, J. T. 2003, *PASP*, 115, 389
 Young, J. S., & Scoville, N. Z. 1984, *ApJ*, 287, 153
 Yun, M. S., Ho, P. T. P., & Lo, K. Y. 1993, *ApJ*, 411, L17